Precessing rotating flows with additional shear: Stability analysis

A. Salhi[1,2] and C. Cambon[2]
[1]*Département de Physique, Faculté des Sciences de Tunis, 1060, Tunis, Tunisia*
[2]*Laboratoire de Mécanique des Fluides et d'Acoustique, Ecole Centrale de Lyon, UMR 5509 CNRS, INSA, UCB, 69134 Ecully Cedex, France*

(Received 25 July 2008; revised manuscript received 27 November 2008; published 12 March 2009)

We consider unbounded precessing rotating flows in which vertical or horizontal shear is induced by the interaction between the solid-body rotation (with angular velocity Ω_0) and the additional "precessing" Coriolis force (with angular velocity $-\varepsilon\Omega_0$), normal to it. A "weak" shear flow, with rate 2ε of the same order of the Poincaré "small" ratio ε, is needed for balancing the gyroscopic torque, so that the whole flow satisfies Euler's equations in the precessing frame (the so-called admissibility conditions). The base flow case with vertical shear (its cross-gradient direction is aligned with the main angular velocity) corresponds to Mahalov's [Phys. Fluids A **5**, 891 (1993)] precessing infinite cylinder base flow (ignoring boundary conditions), while the base flow case with horizontal shear (its cross-gradient direction is normal to both main and precessing angular velocities) corresponds to the unbounded precessing rotating shear flow considered by Kerswell [Geophys. Astrophys. Fluid Dyn. **72**, 107 (1993)]. We show that both these base flows satisfy the admissibility conditions and can support disturbances in terms of advected Fourier modes. Because the admissibility conditions cannot select one case with respect to the other, a more physical derivation is sought: Both flows are deduced from Poincaré's [Bull. Astron. **27**, 321 (1910)] basic state of a precessing spheroidal container, in the limit of small ε. A Rapid distortion theory (RDT) type of stability analysis is then performed for the previously mentioned disturbances, for both base flows. The stability analysis of the Kerswell base flow, using Floquet's theory, is recovered, and its counterpart for the Mahalov base flow is presented. Typical growth rates are found to be the same for both flows at very small ε, but significant differences are obtained regarding growth rates and widths of instability bands, if larger ε values, up to 0.2, are considered. Finally, both flow cases are briefly discussed in view of a subsequent nonlinear study using pseudospectral direct numerical simulations, which is a natural continuation of RDT.

DOI: 10.1103/PhysRevE.79.036303 PACS number(s): 47.27.W−, 47.20.Cq, 47.27.Gs

I. INTRODUCTION

Rotating fluids can develop specific "precession" instabilities if they are subjected to an additional weak external Coriolis force. Such instabilities were recently shown to trigger a new route to turbulence with enhancement of mixing. In addition, very promising occurrence and sustenance of dynamo effects are expected in magnetohydrodynamics. In this context, experimental, theoretical, and numerical studies have been carried out in both spherical [1] and cylindrical [2] geometries. In the latter case, the linear stability of a rotating fluid column, with the precessing angular velocity normal to the main one, was investigated in [3], by means of a classical normal mode analysis of small disturbances.

We propose in this paper to use a different approach to linear stability: Disturbances to a simple base flow are sought in terms of three-dimensional Fourier modes that are passively advected by this base flow; consequently they involve a time-dependent wave vector in addition to a time-dependent amplitude. This approach was illustrated in, e.g., [4,5] in the field of hydrodynamic stability, but it is also the starting point of the rapid distortion theory (RDT), as coined by Batchelor and Proudman [6], used in the turbulence community. Comparison of this RDT approach to the conventional (normal mode) one is encouraged by previous "success stories," including elliptical flow instability [4,7,8] and rotating flow with weak axial periodic compression [9,10]. Directly relevant to the problem with precession and shear is the special case of the Poincaré spheroidal container addressed by Kerswell [11], who performed a RDT-like stability analysis for a special case. Going back to the stability analysis of Mahalov [3], only the conventional normal mode analysis was done, but it is possible to define a base flow with constant velocity gradients, ignoring specific boundary conditions. Both base flows, hereinafter referred to as Mahalov base flow (MBF) and Kerswell base flow (KBF) are exact solutions of Euler equations, and can support disturbances in terms of advected Fourier modes. These two flows, however, differ in their pure shear part, as we will see in Sec. II, and this raises at least two questions, which motivate our present study. On the one hand, is there a physical derivation of these flows, if admissibility conditions, as we will show in Sec. II, are not sufficient to distinguish them? On the other hand, are there significant differences in their stability (growth rates, widths of instability bands)?

This paper is organized as follows. In Sec. II, "linear and extensional" base flows are introduced and discussed. RDT equations for disturbances are derived in Sec. III, and are exploited analytically and numerically. Sec. IV is devoted to conclusions and perspectives.

II. EXTENSIONAL LINEAR BASE FLOWS

A. Admissibility conditions

A base flow which consists of a solid-body rotation is not a solution of the Euler equations in the presence of an addi-

tional Coriolis force, if the two angular velocities are not aligned. The related gyroscopic torque, which will be subsequently formalized [Eq. (4), first term], needs to be balanced by another velocity gradient term. Let us start with an unspecified additional gradient matrix $\boldsymbol{S}$, in order to determine the necessary constraints on it that result from admissibility conditions (following the terminology of Craik [5]). The base flow with uniform velocity gradients, sometime called linear and/or extensional, is therefore chosen as

$$A_{ij} = \epsilon_{ijn}\Omega_n + S_{ij}, \tag{1}$$

where ϵ_{ijn} is the third-order alternating (sometimes referred to as the Levi-Cività) tensor. The flow is seen in a frame rotating with angular velocity $\boldsymbol{\Omega}^c$ (superscript c for Coriolis). The admissibility conditions can be most easily seen from the Helmholtz equation in the rotating frame (e.g., [12]),

$$\partial_t \boldsymbol{W} + \boldsymbol{U}\cdot\boldsymbol{\nabla}\boldsymbol{W} = \boldsymbol{A}\cdot\boldsymbol{W} + \nu\nabla^2\boldsymbol{W}, \tag{2}$$

for the basic absolute vorticity $\boldsymbol{W}=\boldsymbol{\nabla}\times\boldsymbol{U}+2\boldsymbol{\Omega}^c$, or

$$W_i = \epsilon_{ijn}S_{nj} + 2\Omega_i + 2\Omega_i^c. \tag{3}$$

Equation (2) reduces to a condition of zero production of absolute vorticity, or $A_{ij}W_j=0$, because the time derivative $\partial_t\boldsymbol{W}$, advection $\boldsymbol{U}\cdot\boldsymbol{\nabla}\boldsymbol{W}$, and viscous term $\nu\nabla^2\mathbf{W}$ disappear for a time-independent linear base flow. From Eqs. (1) and (2), the production of absolute vorticity appears to have four distinct contributions:

$$A_{ij}W_j = \underbrace{2\epsilon_{ijn}\Omega_j\Omega_n^c}_{1} + \underbrace{(S_{ij}+S_{ji})\Omega_j}_{2} + \underbrace{2S_{ij}\Omega_j^c}_{3} + \underbrace{\epsilon_{jpq}S_{ij}S_{qp}}_{4}.$$

It is now clear that the previously mentioned gyroscopic torque is the first term in the right-hand side, and that $\boldsymbol{S}$ is involved in all the other terms for possible balance (the admissibility conditions are violated without $\boldsymbol{S}$). Restricting $\boldsymbol{S}$ to a pure plane shear, the last shear-shear interaction term is zero, so that the admissibility condition yields

$$2\boldsymbol{\Omega}\times\boldsymbol{\Omega}^c + (\boldsymbol{S}+\boldsymbol{S}^T)\cdot\boldsymbol{\Omega} + 2\boldsymbol{S}\cdot\boldsymbol{\Omega}^c = \mathbf{0}. \tag{4}$$

We will consider now the case where $\boldsymbol{\Omega}$ and $\boldsymbol{\Omega}^c$ are perpendicular. Without lack of generality, the axes of the Cartesian frame of reference can be chosen so that

$$\boldsymbol{\Omega} = [0,0,\Omega_0]^T, \quad \boldsymbol{\Omega}^c = [\Omega^c,0,0]^T, \tag{5}$$

in which the superscript T means the matrix transpose. Accordingly, one easily shows that only the following base shear flows satisfy Eq. (4):

$$\boldsymbol{S} = \begin{bmatrix} 0 & 0 & 0 \\ -\Omega_0 & 0 & 0 \\ 0 & 0 & 0 \end{bmatrix}, \quad \begin{bmatrix} 0 & 0 & 0 \\ 0 & 0 & -2\Omega^c \\ 0 & 0 & 0 \end{bmatrix}, \quad \begin{bmatrix} 0 & 0 & 0 \\ 0 & 0 & 0 \\ 0 & -2\Omega^c & 0 \end{bmatrix},$$

but only the last two cases are relevant for the present study, because a plane shear, with shear rate independent of the Coriolis force, is recovered for the first case. The last two base flows are seen in a precessing frame, and therefore subject to a Coriolis force, which is characterized by the second angular velocity in Eq. (5). Choosing

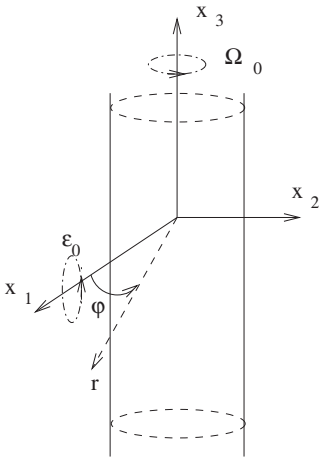

FIG. 1. Sketch for Mahalov's base flow.

$$\Omega^c = \varepsilon\Omega_0, \tag{6}$$

the Poincaré number [1,13] ε could be considered as a small parameter: It is really very small in the geophysical context ($\sim 10^{-7}$), but significant values up to 0.2 are displayed in typical experimental studies to trigger instabilities and turbulence [1,2]. Finally, the two relevant base flows are

$$\boldsymbol{U} = \Omega_0\begin{bmatrix} 0 & -1 & 0 \\ 1 & 0 & 0 \\ 0 & -2\varepsilon & 0 \end{bmatrix}\cdot\boldsymbol{x}, \quad \boldsymbol{U} = \Omega_0\begin{bmatrix} 0 & -1 & 0 \\ 1 & 0 & -2\varepsilon \\ 0 & 0 & 0 \end{bmatrix}\cdot\boldsymbol{x}. \tag{7}$$

They reduce to a solid-body rotation in the absence of the Coriolis force, and the shear can be seen as generated by the interaction between the Coriolis force and the solid-body rotation.

For the first of these basic flows (hereinafter referred to as MBF), the streamwise direction of shear is along $\boldsymbol{\Omega}$ (vertical here, see Fig. 1) and the absolute vorticity $\boldsymbol{W}=[0,0,2\Omega_0]^T$ is not affected by the precession. In counterpart, for the second base flow (hereinafter referred to as KBF), it is the cross-gradient direction of the shear that is vertical (along $\boldsymbol{\Omega}$), and an additional component of absolute vorticity $\boldsymbol{W}=[4\varepsilon\Omega_0,0,2\Omega_0]^T$ arises along $\boldsymbol{\Omega}^c$.

B. Derivation of the base flows from Poincaré's basic state at weak precession

The Poincaré base state of a precessing spheroidal container [13], reconsidered by Kerswell [11], is

$$\boldsymbol{U} = \Omega_0\begin{bmatrix} 0 & -1 & 0 \\ 1 & 0 & -(1+\eta)\mu \\ 0 & \mu & 0 \end{bmatrix}\boldsymbol{x} = \boldsymbol{A}\cdot\boldsymbol{x}, \tag{8}$$

where

$$\mu = \frac{2\varepsilon_1}{\eta + 2(1+\eta)\varepsilon_3}, \tag{9}$$

and η is the oblateness of the spheroidal container $|\boldsymbol{r}|^2 + \eta(\boldsymbol{e}_3\cdot\boldsymbol{r})^2=1$ with the two-component precessional vector $\boldsymbol{\Omega}^c=\Omega_0[\varepsilon_1,0,\varepsilon_3]^T$.

It is clear that the MBF cannot be recovered from Eqs. (8) and (9) by simply discarding ε_3 and choosing $\eta=0$ (circular cylinder). It is necessary to rotate the system of coordinates in the plane x_1-x_3 in order to eliminate the nonzero component A_{23} in (8). Accordingly, in the new system of coordinates $(\tilde{x}_1,\tilde{x}_2,\tilde{x}_3)$ such that

$$\begin{bmatrix} \tilde{x}_3 \\ \tilde{x}_1 \\ \tilde{x}_2 \end{bmatrix} = \frac{1}{\sqrt{1+\gamma^2}} \begin{bmatrix} 1 & \gamma & 0 \\ -\gamma & 1 & 0 \\ 0 & 0 & \sqrt{1+\gamma^2} \end{bmatrix} \begin{bmatrix} x_3 \\ x_1 \\ x_2 \end{bmatrix}, \tag{10}$$

where $\gamma=\tan(\tilde{x}_3\hat{,}x_3)$, the basic velocity gradient and the precessional angular velocity vector take the following forms:

$$\tilde{\boldsymbol{A}} = \frac{\Omega_0}{\sqrt{1+\gamma^2}} \begin{bmatrix} 0 & -[1+\mu\gamma] & 0 \\ [1+(1+\eta)\mu\gamma] & 0 & [\gamma-(1+\eta)\mu] \\ 0 & [\mu-\gamma] & 0 \end{bmatrix},$$

$$\tilde{\boldsymbol{\Omega}}^c = [\tilde{\varepsilon}_1,0,\tilde{\varepsilon}_3]^T = (1+\gamma^2)^{-1/2}[\varepsilon_1-\gamma\varepsilon_3,0,\gamma\varepsilon_1+\varepsilon_3]^T. \tag{11}$$

Choosing $\gamma=(1+\eta)\mu$, the coefficient $\tilde{A}_{23}$ vanishes in (11) and the matrix $\tilde{\boldsymbol{A}}$ reduces to

$$\tilde{\boldsymbol{A}} = \Omega_0 \begin{bmatrix} 0 & -\chi & 0 \\ \chi & 0 & 0 \\ 0 & -\eta\mu/\chi & 0 \end{bmatrix}, \tag{12}$$

where

$$\chi = [1+(1+\eta)^2\mu^2]^{1/2}. \tag{13}$$

By neglecting the terms of order $O(\mu^\ell)$ with $\ell>1$ and assuming that

$$\tilde{\varepsilon}_3 = (1+\eta)\mu\varepsilon_1 + \varepsilon_3 = 0,$$

so that

$$\tilde{\varepsilon}_1 = \varepsilon_1 - \gamma\varepsilon_3 = [1+(1+\eta)^2\mu^2]\varepsilon_1 = \varepsilon_1 + O(\mu^2),$$

we obtain the MBF described by the first matrix in Eqs. (7) and (6) with $\eta\mu=2\varepsilon_1=2\varepsilon$.

It is worthwhile to stress that the geometry of the oblate spheroid does not provide in a trivial way the relevant parameter (e.g., zero oblateness for a circular cylinder) to recover the MBF. A rotation of the system of coordinates is needed to discard both the component of the precessional angular velocity that is along the main angular velocity, and one of the extra-diagonal components of the gradient matrix. The choice of the base flow by Mahalov was also suggested by Wiener *et al.* [14], who studied experimentally the stability of (horizontal) Taylor-Couette flow subject to an external (vertical) Coriolis force. They showed that the Coriolis force alters the flow field in generating an axial component for the basic velocity.

If $\gamma=\mu$, as firstly stated by Kerswell [11], the coefficient $\tilde{A}_{32}$ vanishes in (11), and one recovers Eqs. (1.1) and (1.2) in [11]. In addition, by neglecting the terms of order $O(\mu^\ell)$ with $\ell>1$ and assuming that $\tilde{\varepsilon}_3=\mu\varepsilon_1+\varepsilon_3=0$, so that $\tilde{\varepsilon}_1=\varepsilon_1+O(\mu^2)$, we recover the KBF described by the second matrix in (7) and Eq. (6) [or Eq. (5.1) in [11]] with $\varepsilon_1=\varepsilon=\eta\mu$.

III. STABILITY ANALYSIS

A. Brief comments about effects of rotation and shear, coupled or not

Solid-body rotation does not produce energy but generates dispersive inertial waves, which can alter intercomponent and interscale energy distribution by linear effects of phase mixing and nonlinear dynamics (e.g., inertial wave turbulence) [12,15]. On the other hand, the mean shear produces energy but only algebraic growth is obtained in the absence of rotation. An important effect of the shear is to quench transport: this can be seen from the calculation of a turbulent eddy-viscosity term from the RDT solution [16], not to mention the "sheltering effect" studied by Hunt in the context of inhomogeneous turbulence. In the case of shear (rate S) rotating (rate Ω) around its spanwise direction, exponential instability is found for anticyclonic cases $-1<\Omega/S<0$. The relevance of a simple criterion that accounts only for production of kinetic energy is explained by the role of pressure-released modes [17]. Details of RDT can be found in [18,19], with recent applications in the context of astrophysics in [16,20,21]. A crucial point in all cases with mean shear is the possibility of promoting exponential growth by feeding the vertical (cross-gradient) velocity component by means of a coupled effect (rotation, stratification), or even by nonlinear redistribution terms. In the present case, the main difference from other rotating shear flows is the fact that the mean trajectories and related characteristic curves are no longer the ones for the pure shear, which are rectilinear unbounded curves, but are also affected by the main rotation, so that the trajectories are ellipses and the eikonal equation has time-periodic solutions. In this sense, we are closer to elliptical flow instability, in which rotation is coupled with weak additional irrotational strain than to the barotropic instability of rotating shear. The equations of mean flow trajectories are not given for the sake of brevity. They are closely related to characteristic curves in wave space, comparing the trajectory equation to the eikonal equation, changing (x_i,X_j,A_{ij}) into $(k_i,K_j,-A_{ji})$. Accordingly, the MBF trajectories, shown in Fig. 2 are equivalent to KBF spectral characteristic curves, and conversely (see Fig. 3 for KBF trajectories.)

B. Equations for disturbances

The solutions for the disturbances to the base flow are found in the form of single plane waves with a time-dependent wave vector,

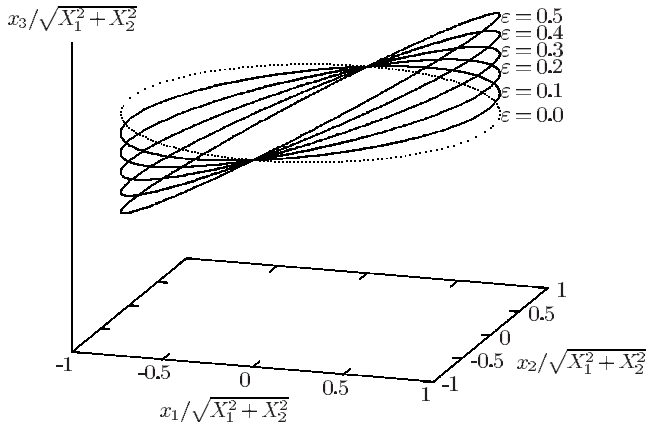

FIG. 2. Trajectories in physical space for the MBF at $X_3=2\varepsilon X_1$ and $\varepsilon=0.0-0.5$ with increments of 0.1.

$$[\boldsymbol{u}(\boldsymbol{x},t),p(\boldsymbol{x},t)]=[\hat{\boldsymbol{u}}(\boldsymbol{k},t),\hat{p}(\boldsymbol{k},t)]\exp(\imath\boldsymbol{k}(t)\cdot\boldsymbol{x}). \quad (14)$$

The following linear system of ordinary differential equations (ODEs) is found:

$$\frac{d\hat{u}_i}{dt}+\left(\delta_{in}-2\frac{k_ik_n}{k^2}\right)A_{nj}\hat{u}_j+\varepsilon\left(\delta_{in}-\frac{k_ik_n}{k^2}\right)\epsilon_{n1j}\Omega\hat{u}_j=0, \quad (15)$$

in terms of $\hat{\boldsymbol{u}}$, once the pressure term is eventually solved in order to satisfy $\boldsymbol{k}\cdot\hat{\boldsymbol{u}}=0$, according to the incompressibility constraint (see, e.g., [15,18]). Linearity is implicit if a single-mode disturbance is considered, because such a mode cannot interact with itself. Only in the context of conventional RDT ought linearization to be imposed as an assumption because the disturbance is multimodal. As a key point to account for advection by the base flow, the time derivative in the preceding equation involves the time dependency of the wave vector, in accordance with the following (eikonal-type) wave vector equation:

$$d\boldsymbol{k}/dt=-\boldsymbol{A}^T\boldsymbol{k}. \quad (16)$$

C. Characteristic curves in wave space

For the MBF, the eikonal equation reduces to

$$\dot{k}_1=-k_2,$$

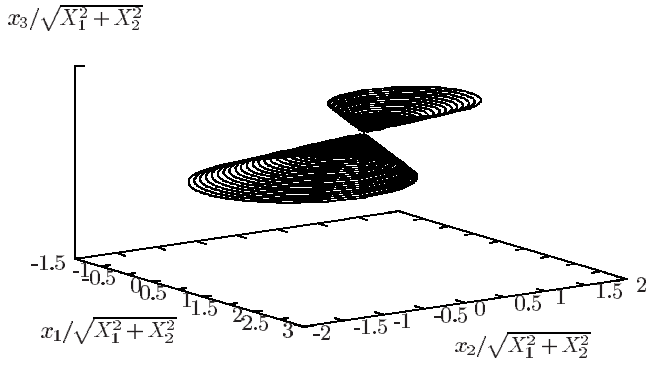

FIG. 3. Trajectories in physical space for the KBF at $\varepsilon=0.1$, $X_2=0$, and $-1\leqslant(X_3/X_1)\leqslant 9$.

$$\dot{k}_2=k_1+2\varepsilon k_3,$$

$$\dot{k}_3=0,$$

with solutions

$$k_3=K_3,$$

$$k_1+2\varepsilon k_3=(K_1+2\varepsilon K_3)\cos\tau-K_2\sin\tau,$$

$$k_2=(K_1+2\varepsilon K_3)\sin\tau+K_2\cos\tau, \quad (17)$$

where the capital letter $\boldsymbol{K}$ denotes the initial value, as $\boldsymbol{X}$ does for the trajectories in Figs. 2 and 3.

In general, the inviscid RDT solutions depend on the orientation, not on the modulus, of the wave vector. Consequently, these solutions must be parametrized by two angles, which are, for instance, the angles of the initial wave vector $\boldsymbol{K}$ in a system of spherical coordinates. A better (simpler) parametrization can be found here because the characteristic lines (or "trajectories" in wave space) exhibit two invariants, namely,

$$k_3=K_3,\quad (k_1+2\varepsilon k_3)^2+k_2^2=(K_1+2\varepsilon K_3)^2+K_2^2, \quad (18)$$

which define ellipses in wave space. In this case, a simpler form of the characteristic lines is found if the wave numbers are expressed in terms of the three independent variables k_0, α (combining the two previous invariants), and t^*,

$$k_0=K_3,\quad \alpha=\arctan\left(\frac{\sqrt{K_2^2+(K_1+2\varepsilon K_3)^2}}{K_3}\right), \quad (19)$$

$$k_0\tan\alpha=\sqrt{K_1^2+K_2^2},$$

$$t^*=\Omega_0 t+\arctan\left(\frac{K_2}{K_1+2\varepsilon K_3}\right). \quad (20)$$

Thus

$$k_1=k_0(\tan\alpha\cos t^*-2\varepsilon),$$

$$k_2=k_0\tan\alpha\sin t^*,$$

$$k_3=k_0. \quad (21)$$

It is clear that k_0 can be removed from consideration for further stability analysis, because it affects only the modulus of the wave vector; accordingly, only the single angular parameter α and the external parameter ε are needed to analyze the stability. Introduction of the variables k_0 and α is not relevant in the case $k_3=K_3=0$: This exception does not affect the analysis of exponential instability, because there is marginal stability for $K_3=0$.

For the KBF, the solutions of the eikonal equation display the two invariants

$$k_1^2+k_2^2=K_1^2+K_2^2,\quad k_3+2\varepsilon k_1=K_3+2\varepsilon K_1, \quad (22)$$

defining ellipses. As for the MBF, the following simplified form is recovered [Eq. (5.4) in Kerswell [11]]:

$$k_1 = k_0 \tan\alpha \cos t^*,$$

$$k_2 = k_0 \tan\alpha \sin t^*,$$

$$k_3 = k_0(1 - 2\varepsilon \tan\alpha \cos t^*), \tag{23}$$

with

$$t^* = \Omega_0 t + \arctan\left(\frac{K_2}{K_1}\right) = \Omega_0 t + \varphi,$$

$$\alpha = \arctan\left(\frac{\sqrt{K_1^2 + K_2^2}}{K_3 + 2\varepsilon K_1}\right) = \arctan\left(\frac{\tan\theta}{1 + 2\varepsilon \tan\theta \cos\varphi}\right),$$

$$k_0 = k_3 + 2\varepsilon k_1 = K_3 + 2\varepsilon K_1,$$

$$k_0 \tan\alpha = \sqrt{k_1^2 + k_2^2} = \sqrt{K_1^2 + K_2^2} = K \sin\theta.$$

For convenience, the angles θ (polar) and φ (azimuthal) of $\boldsymbol{K}$ in a system of polar-spherical coordinates of polar axis $\boldsymbol{e}_3$ are used too.

The stability analysis here is obtained by solving an initial value problem. In addition to the external parameter ε, the results of this analysis depend only on the initial orientation of the wave vector, as the only characteristic of different initial values for the disturbances. The single parameter α is shown to give a parametrization of the orientation of the initial wave vector that is simpler than the one in terms of the two angles θ and φ, because of the existence of two invariants in the characteristic curves (trajectories in Fourier space).

A more physical interpretation of the angular parameter α can be offered as follows. In typical experiments in a rotating tank with local forcing, cross-shaped structures, often called Saint Andrew crosses, reflect the generation of inertial waves by means of conical rays emanating from the forcing zone. The angle, similar to α, that characterizes the cross-shaped structure with respect to the axis of rotation, can be predicted in equating the dispersion frequency, say $\pm 2\Omega \cos\alpha$, to the forcing frequency σ_0, so that it is given by $\cos\alpha = \pm\sigma_0/(2\Omega)$ provided that $\sigma_0 < 2\Omega$. Elliptical instability at weak ellipticity can be explained by a similar, parametric, resonance, when the dispersion frequency of an inertial wave is approximately equal to the frequency of the periodic motion Ω of the wave vector resulting from the eikonal equation, so that $\cos\alpha = \pm 1/2$ is selected according to the strongest resonance condition. In this case, growth of instability results from the averaged (over a period) alignment of the fluctuating vorticity with the principal axis of the weak additional strain (see also [7,15] for more details.)

D. Use of a minimal number of components for the velocity disturbances in wavespace

Equation (17) is a system of three linear ODEs, for $\hat{u}_1$, $\hat{u}_2$, and $\hat{u}_3$, these three components being coupled by the condition $\boldsymbol{k}\cdot\hat{\boldsymbol{u}} = 0$. One of the simplest and more systematic ways to write the equations for a minimal number of dependent variables is to project $\hat{\boldsymbol{u}}$ in a local frame of reference

$$\boldsymbol{e}^{(1)} = \boldsymbol{k} \times \boldsymbol{n}/\|\boldsymbol{k} \times \boldsymbol{n}\|, \quad \boldsymbol{e}^{(2)} = \boldsymbol{k} \times \boldsymbol{e}^{(1)}/k, \quad \boldsymbol{e}^{(3)} = \boldsymbol{k}/k, \tag{24}$$

so that $\hat{\boldsymbol{u}}$ has only two components,

$$\hat{\boldsymbol{u}} = u^{(1)}\boldsymbol{e}^{(1)} + u^{(2)}\boldsymbol{e}^{(2)}, \tag{25}$$

and the incompressibility condition is implied. Of course, the local frame, often called the Craya-Herring frame in the turbulence community, is the local frame attached to a system of polar-spherical coordinates for $\boldsymbol{k}$ with polar axis $\boldsymbol{n}$. The choice $\boldsymbol{n} = \boldsymbol{e}_3$ is consistent with axial symmetry at vanishing ε, without being restricted to this case. Accordingly, Eq. (15) yields the following system of two equations for $u^{(1)}$ and $u^{(2)}$ (subsequently called "toroidal" and "poloidal" in reference to their meaning in physical space [15]):

$$\frac{d}{dt^*}\begin{bmatrix} u^{(1)} \\ u^{(2)} \end{bmatrix} + \underbrace{\begin{bmatrix} m_{11} & m_{12} \\ m_{21} & m_{22} \end{bmatrix}}_{\boldsymbol{m}} \begin{bmatrix} u^{(1)} \\ u^{(2)} \end{bmatrix} = \begin{bmatrix} 0 \\ 0 \end{bmatrix}. \tag{26}$$

General solutions of Eq. (26) can be written as

$$u^{(\alpha)}(\boldsymbol{k}(t), t) = g_{\alpha\beta}(\boldsymbol{k}, t, 0) u^{(\beta)}(\boldsymbol{K}, 0), \tag{27}$$

in which the reduced Green's function $g_{\alpha\beta}$ (greek indices take only the values 1 and 2) is governed by the same equation as $u^{(\alpha)}$ is, but with universal initial condition $\boldsymbol{g}(0) = \boldsymbol{I}_2$, where $\boldsymbol{I}_2$ is the 2×2 unit matrix.

E. Stability analysis: analytical results

For the MBF, the matrix $\boldsymbol{m}$ takes the following form:

$$\boldsymbol{m} = \frac{2}{k}\begin{bmatrix} 0 & -k_3 \\ (k_3 - \varepsilon k_1) & \varepsilon(k_2 k_3/k) \end{bmatrix} = \frac{2}{k}\begin{bmatrix} 0 & -k_0 \\ (k_0 - \varepsilon k_1) & \varepsilon(k_2 k_3/k) \end{bmatrix}. \tag{28}$$

Trivial solutions of (26) are found if the wave vector is no longer time dependent in (28); these solutions gives purely oscillating or constant motion and correspond to $\alpha = 0$ or $\pi/2$, with

$$g_{11}(t) = \cos\sigma t, \quad g_{12}(t) = (1 + 2\varepsilon^2)^{-1/2} \sin\sigma t,$$

$$g_{21}(t) = -(1 + 2\varepsilon^2)^{1/2} \sin\sigma t, \quad g_{22}(t) = \cos\sigma t, \tag{29}$$

in which

$$\sigma = 2\Omega_0\left(\frac{k_3^2}{k^2} - \varepsilon\frac{k_1 k_3}{k^2}\right)^{1/2} = 2\Omega_0\left(\frac{1 + 2\varepsilon^2}{1 + 4\varepsilon^2}\right)^{1/2}$$

in the first case, and

$$g_{11} = g_{22} = 1, \quad g_{12} = 0, \quad g_{21} = 2\varepsilon \sin(\Omega_0 t + \varphi) \tag{30}$$

in the second case.

For the KBF, the matrix $\boldsymbol{m}$ in (26) takes the form

$$\boldsymbol{m} = \frac{2}{k}\begin{bmatrix} 0 & -(k_3 + 2\varepsilon k_1) \\ (k_3 + \varepsilon k_1) & \varepsilon(k_2 k_3/k) \end{bmatrix} = \frac{2}{k}\begin{bmatrix} 0 & -k_0 \\ (k_0 - \varepsilon k_1) & \varepsilon(k_2 k_3/k) \end{bmatrix}, \tag{31}$$

in which the wave numbers are described by (23). Similarly

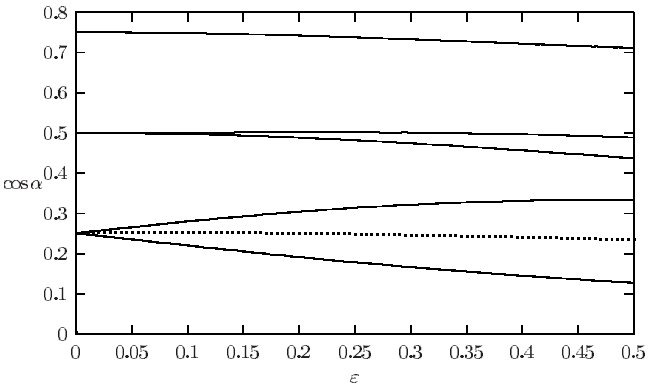

FIG. 4. Instability bands delineated by neutral curves in the $(\varepsilon, \cos\alpha)$ plane, MBF case. The dashed line indicates the inclination α of the largest growth rate.

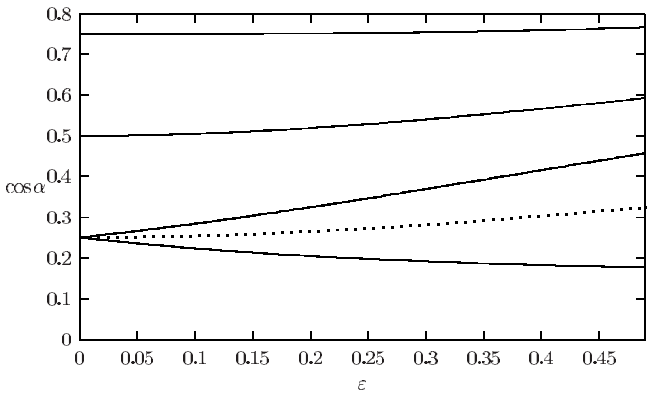

FIG. 5. Instability bands delineated by neutral curves in the $(\varepsilon, \cos\alpha)$ plane, KBF case. The dashed line indicates the inclination α of the largest growth rate.

to the MBF case, simple solutions are found for $\alpha=0$ or $\pi/2$, as

$$g_{11} = g_{22} = \cos\Omega_0 t, \quad g_{21} = -g_{12} = -\sin\Omega_0 t \tag{32}$$

in the first case, and

$$g_{11} = 1, \quad g_{12} = 0,$$

$$g_{21} = 2\varepsilon[1 + 4\varepsilon^2\cos^2(\Omega_0 t + \varphi)]^{-1/2}\sin(\Omega_0 t + \varphi),$$

$$g_{22} = \left(1 + 4\varepsilon^2\frac{K_1^2}{K_1^2 + K_2^2}\right)^{1/2}[1 + 4\varepsilon^2\cos^2(\Omega_0 t + \varphi)]^{-1/2} \tag{33}$$

in the second case. It should be remarked that, at $|\varepsilon| \ll 1$, the solution (29) [(33)] reduces to (32) [(30)]. The coincidence of the stability analysis for both base flows at sufficiently weak precession is confirmed as follows.

1. Stability analysis at sufficiently weak precession

When $\alpha \neq 0, \pi/2$ and $|\varepsilon| \ll 1$, the stability problem for both the MBF and the KBF is governed by the following Mathieu equation deduced from the system (27), with (28) and (31),

$$\frac{d^2Y}{dt^{*2}} + (a_0^2 - 2\varepsilon a_1\cos t^*)Y = 0, \quad Y = (k/K)u^{(1)}, \tag{34}$$

$$a_0^2 = 4\cos^2\alpha, \quad a_1 = (3 - 2a_0^2)\cos\alpha\sin\alpha, \tag{35}$$

with more details in the Appendix. The dominant coefficient in this equation is a_0 which coincide with the nondimensional dispersion frequency of inertial waves $2k_1/k = 2k\cos\theta$ at weak ε, displaying the precession instability as a parametric instability of inertial waves. The stability properties of the Mathieu equation are well known [22]. For small ε, the solutions are generally bounded, except in the vicinity of resonances defined by

$$a_0^2 = 4\cos^2\alpha = n^2/4, \quad n = 1,2,3,4, \tag{36}$$

where the solutions are exponentially growing with a growth rate of order ε^n. Equation (36) implies that there are four instability bands that are centered at $a_0^2 = 0.25, 1, 9/4, 4$, respectively. However, since the width of the last three unstable bands is of $O(\varepsilon^n)$ with $n > 1$, the Mathieu equation is not able to determine whether instability exists near $a_0^2 = 1, 9/4, 4$ for the original system (27). Moreover, in contrast to Eq. (36), the solution (29) [or (32)] clearly shows that the mode $\alpha=0$, so that $a_0^2=4$, is stabilizing. Consequently, Eq. (36) characterizes only the subharmonic state $(n=1)$ at sufficiently small $|\varepsilon|$ (see the Appendix). By using the power statement

$$\frac{d}{dt^*}(|\hat{\boldsymbol{u}}|^2) = 2\varepsilon\hat{u}_2\hat{u}_3,$$

obtained through the dot product of $\hat{\boldsymbol{u}}$ with Eq. (15), Kerswell [11] demonstrated that, in the limit of $\varepsilon \to 0$, the maximal growth rate of the subharmonic instability is $\sigma_m^*/\varepsilon = 5\sqrt{15}/32$. The above result can be recovered by considering the stability properties of the Mathieu equation (see the Appendix).

F. Numerical results using Floquet's technique and discussion

The temporal behavior of the solutions is obtained using Floquet theory allied to numerical computations. From $d/dt(\mathrm{Det}\boldsymbol{g}) + m_{\alpha\alpha}\mathrm{Det}\boldsymbol{g} = 0$, it is found that $\mathrm{Det}\boldsymbol{g} = k/K$, and therefore is equal to 1 at any period. Consequently, the two Floquet multipliers, which are the eigenvalues of $\boldsymbol{g}$ after a period, are either real with the form $\{\lambda, 1/\lambda\}$, or are complex conjugates lying on the unit circle. Accordingly, the only quantity we need to know in order to compute the two relevant eigenvalues is the trace of the matrix $\boldsymbol{g}$ after one period. Instability, with a growth rate σ^*, is found for

$$|\Delta| = |g_{\alpha\alpha}(2\pi)| > 2, \quad \sigma^* = \frac{1}{2\pi}\ln\left(\frac{|\Delta| + \sqrt{\Delta^2 - 4}}{2}\right).$$

In addition, the method allows simple generalization to viscous flows, by adding the term $\nu k^2\hat{\boldsymbol{u}}$ in (15), with ν the kinematic viscosity. The viscous solution is derived from the inviscid one by multiplying by the factor $\exp[-\nu\int_0^t k^2(t')dt'] = \exp[-2\pi\sigma_v^*(t^*)]$, where

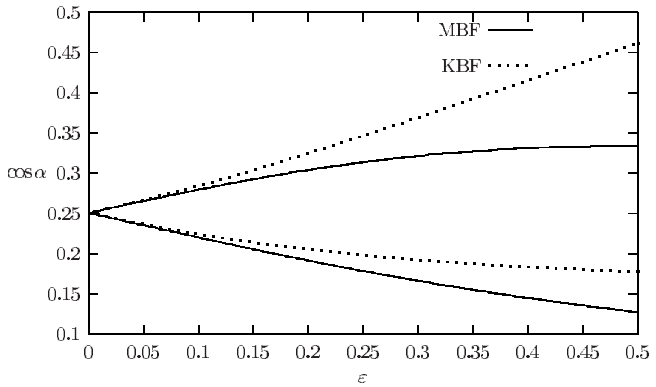

FIG. 6. Subharmonic instability band in the cases of MBF and KBF.

$$\sigma_v^*(2\pi) = E(1 + \tan^2 \alpha + 4\varepsilon^2) \tag{37}$$

for the MBF and

$$\sigma_v^*(2\pi) = E[1 + (1 + 2\varepsilon^2)\tan^2 \alpha] \tag{38}$$

for the KBF, $E = \nu k_0^2/\Omega_0$ being the Ekman number based on the frequency Ω_0. Therefore, in the viscous case, the curve of marginal stability is characterized by $\sigma_t^* = \sigma^* - \sigma_v^* = 0$, or equivalently by $|\Delta| = 2\cosh(2\pi\sigma_v^*)$.

The system (26) is integrated numerically over one period using a fourth-order Runge-Kutta scheme with nondimensional time step $\delta t^* = 10^{-4}\pi$ to find $|g_{\alpha\alpha}|$ for $0 \leqslant \cos\alpha \leqslant 1$ and $0 \leqslant \varepsilon \leqslant 1/2$.

Figures 4 and 5 show the neutral curves which correspond to a constant (small) growth rate 10^{-5} where the horizontal axis is $\varepsilon \leqslant 0.5$ and the vertical axis is $\cos\alpha$. The results for the MBF are displayed in Fig. 4, and those for the KBF are displayed in Fig. 5. In agreement with the numerical results by Kerswell [11], there are three unstable bands (labeled $n = 1-3$) emanating from the points $\cos\alpha = 0.25, 0.50, 0.75$, respectively, located on the $\varepsilon = 0$ axis. The subharmonic instability ($n = 1$) that emanates from the point (0, 0.25), in agreement with Eq. (36), is much the strongest and is extensive. Figure 6 compares the subharmonic instability band in the MBF with that in the KBF. As expected, for $0 \leqslant \varepsilon < 0.1$, the subharmonic instability is the same for both the MBF and KBF. However, for $0.1 < \varepsilon$, that in the KBF is larger, and its maximal growth rate remains larger, too, as shown by Fig. 7.

While for the KBF both the second and the third instabilities are very thin (so they reduce to the lines shown in Fig. 5), for the MBF only the third instability is very thin. The second instability band in the MBF case is less important than the subharmonic one, but it is not as narrow as that in the KBF case. As shown by Fig. 8 displaying the growth rate σ^* versus $\cos\alpha$ at $\varepsilon = 0.5$, the value of the maximal growth rate of the second instability in the MBF case is not small with respect to that of the subharmonic instability.

The viscous classical normal-mode analysis by Mahalov shows that the transition between stability and instability is characterized by $\varepsilon = 0.158$, in agreement with his full numerical simulations of the Navier-Stokes equations at $R_e = \Omega_0(R_2 - R_1)^2/\nu = 300$ and $R_1/R_2 = 0.5$, where R_1 and R_2 are

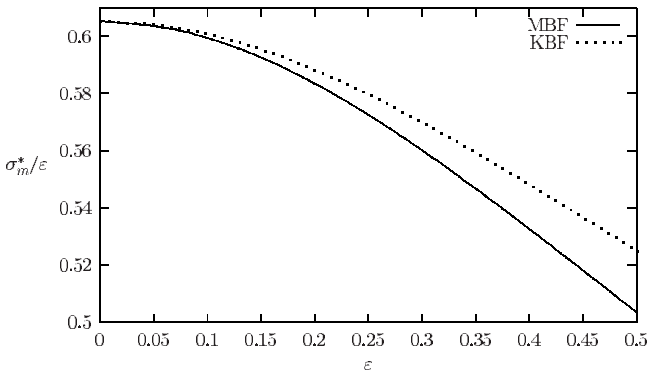

FIG. 7. Variation of σ_m^*/ε (maximal growth rate normalized by ε) versus ε for the MBF and KBF (dashed line) cases. In the limit $\varepsilon \to 0$, one has $\sigma_m^*/\varepsilon = 5\sqrt{15}/32$ (see [11]).

the radii of the two rotating coaxial cylinders. Assuming that such a result can be applied in the case of the present stability analysis, for $\varepsilon = 0.158$, we determine numerically both σ_m^* and α_m and we use the relation $\sigma_m^* = \sigma_v^*$ with Eq. (37) or (38) to deduce the value of the Ekman number: $E = 5.73 \times 10^{-3}$ for the MBF and 6.17×10^{-3} for the KBF. Figure 9 shows the variation of σ_m^* and $\sigma_v^*(\alpha_m)$ at $E = 5.73 \times 10^{-3}$ versus ε, displaying stability for $0 \leqslant \varepsilon < 0.158$ and instability for $\varepsilon > 0.158$.

IV. CONCLUSIONS AND PERSPECTIVES

A precessing rotating flow with main angular velocity $\mathbf{\Omega}$ perpendicular to the axis of precession is considered in order to define its limiting case as an extensional base flow, and to perform its stability analysis for disturbances to it, which can be expressed in terms of advected Fourier modes. This study has reconciled the different approaches by Mahalov [3] and Kerswell [11]. Although it was conjectured for a long time that a mean (base) shear flow is induced as a by-product by only the $\mathbf{\Omega}$ and $\mathbf{\Omega}^c$ angular velocities, this shear is not uniquely determined here and two different cases have to be considered. On the one hand, the link of this shear to the gyroscopic torque has been specified in Eq. (4), using admissibility conditions, whereas the right-hand sides of Eqs. (28)

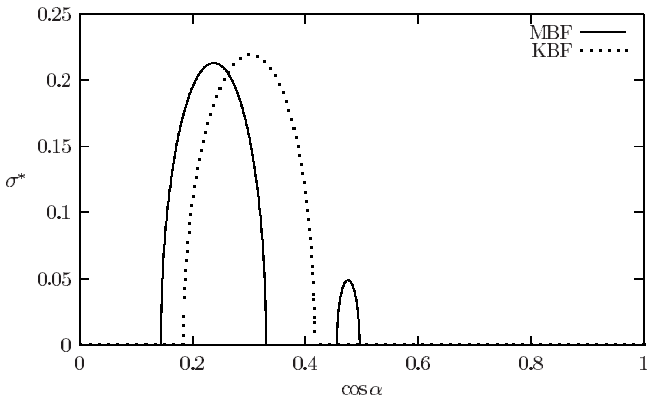

FIG. 8. Variation of the growth rate σ^* of the unstable bands versus $\cos\alpha$ at $\varepsilon = 0.2$ for the MBF and KBF.

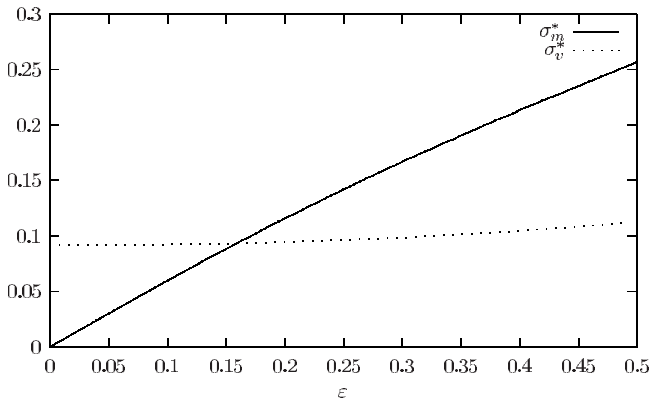

FIG. 9. Variation of inviscid maximal growth σ_m^* and viscous growth σ_v^* [Eq. (27) with $E=5.73\times10^{-3}$] rates versus ε for the case of MBF. The value $E=5.73\times10^{-3}$ has been deduced assuming that the transition between stability and instability occurs at $\varepsilon=0.158$ [3]. For $\sigma_m^*<\sigma_v^*$, viscous effects delay the instability.

and (31) exhibit the same matrix for the analysis of disturbances. On the other hand, the shear–absolute-vorticity interaction is not the same, looking again at Eq. (4), and Eqs. (28) and (31) can differ through implicit time-dependent terms that involve the direction of the wave vector. Both cases, denoted the MBF and KBF, can be derived from the case of the precessing ellipsoid, and one can conjecture that boundary conditions, which are not accounted for in our study, can eventually determine which shear flow is "chosen" by an actual precessing flow. It has been shown that the stability analysis gives the same result for both flows at small Poincaré parameter ε (with $\Omega^c=-\varepsilon\Omega_0$) regarding growth rates and unstable bands, provided that a more intrinsic system of variables [especially α, in Eq. (19) or (23), instead of the polar angle] is used. Significant differences appear, however, at larger ε's. It is expected that the analysis of these analogies and differences will be even more important in a fully nonlinear DNS study, which appears as a natural continuation of our RDT analysis. The present study is also a good opportunity to show the relevance of admissibility conditions and to stress the drawbacks of RDT and DNS studies that do not respect these conditions (e.g., mean shear flow rotating about its vertical axis [23], time-dependent periodic mean shear [24]). The present study will be extended toward pseudospectral DNS in advected coordinates (Rogallo's technique [25]). This technique can incorporate exact mean flow trajectories (elliptical with periodic motion here), whereas it amounts to reintroducing quadratic nonlinear terms such as $u_i\hat{u}_j$ in an equation of type (15). Although these future pseudospectral DNS cannot afford "true" boundary conditions, with some related physical events (ejection of mushroom-shaped eddies from the wall in [2]), some comparisons with structure formation and evolution could be made, as in [26]. For instance, the asymmetry between cyclonic and anticyclonic vortex structures will be investigated in a qualitative and a quantitative way (see also [27]) in both DNS and experimental results, for the precessing flow case.

APPENDIX

For the MBF, system (26) can be rewritten as

$$k\frac{du^{(1)}}{dt^*}=2k_3u^{(2)},$$

$$\frac{d}{dt^*}(ku^{(2)})=-2(k_3-\varepsilon k_1)u^{(1)}.$$

where the relation $(1/k)dk/dt^*=2\varepsilon k_2k_3/k^2$ has been used. An alternative formulation of the last system as a single second-order equation yields,

$$k^2\frac{d^2u^{(1)}}{dt^{*2}}+4\varepsilon k_2k_3\frac{du^{(1)}}{dt^*}+(4k_3^2-4\varepsilon k_1k_3)u^{(1)}=0,$$

and the substitution $Y=(k/K)u^{(1)}$ transforms the above equation to

$$\frac{d^2Y}{dt^{*2}}+V(t^*)Y=0, \tag{A1}$$

where

$$V(t^*)=\left[4\frac{k_3^2}{k^2}-6\varepsilon\frac{k_1k_3}{k^2}-4\varepsilon^2\frac{k_3^2}{k^2}\left(1-\frac{k_2^2}{k^2}\right)\right],$$

which is a Hill equation since the potential is periodic with period 2π. When $0<\varepsilon\ll1$, the potential in (A1) can be expressed by a truncated power series in ε,

$$4k_3^2/k^2=(4\cos^2\alpha)(1+4\varepsilon\sin\alpha\cos\alpha\cos t^*)+O(\varepsilon^2),$$

$$-6\varepsilon k_1k_3/k^2=-6\varepsilon\cos\alpha\sin\alpha\cos t^*+O(\varepsilon^2).$$

If terms of $O(\varepsilon^\ell)$ with $\ell>1$ are neglected, Eq. (A1) reduces to a Mathieu equation [i.e., Eq. (34)],

$$\frac{d^2Y}{dt^{*2}}+(a_0^2-2\varepsilon a_1\cos t^*)Y=0,$$

where a_0^2 and a_1 are given by Eq. (35). For the KBF, the stability problem is also described by (A1) with the potential

$$V(t^*)=4\frac{k_0^2}{k^2}-4\varepsilon\frac{k_1k_0}{k^2}-2\varepsilon\frac{k_1k_3}{k^2}-4\varepsilon^2\frac{k_2^2}{k^2}\left(1-\frac{k_3^2}{k^2}\right),$$

which can be expressed by truncated power series in ε,

$$V(t^*)=a_0^2-2\varepsilon a_1\cos t^*+O(\varepsilon^2),$$

where a_0 and a_1 are also described by Eq. (35). If terms of $O(\varepsilon^\ell)$ with $\ell > 1$ are neglected, one recovers Eq. (34), signifying that, at $\varepsilon \ll 1$, there is the same stability problem for both the MBF and KBF, in agreement with the analysis presented in Sec. III. On the other hand, Eq. (34) implies that the width of the subharmonic instability is $|a_0^2 - 1/4| < |\varepsilon a_1|$, and its maximum growth rate σ_m^* is (in t^* units)

$$\sigma_m^* = |\varepsilon a_1|_{n=1} = |\varepsilon[(3 - 2a_0^2)\cos\alpha \sin\alpha]|_{n=1} = \frac{5\sqrt{15}}{32}|\varepsilon|, \quad \text{(A2)}$$

in the limit of $\varepsilon \to 0$ (see, e.g., [28])

[1] S. Goto, N. Ishii, S. Kida, and M. Nishioka, Phys. Fluids **19**, 061705 (2007).
[2] T. Lehner, W. Mouhali, J. Léorat, and A. Mahalov, Geophys. Astrophys. Fluid Dyn. (to be published).
[3] A. Mahalov, Phys. Fluids A **5**, 891 (1993).
[4] B. J. Bayly, Phys. Rev. Lett. **57**, 2160 (1986).
[5] A. D. D. Craik, J. Fluid Mech. **198**, 275 (1989).
[6] G. K. Batchelor and I. Proudman, Q. J. Mech. Appl. Math. **7**, 83 (1954).
[7] R. R. Kerswell, Annu. Rev. Fluid Mech. **34**, 83 (2002).
[8] R. T. Pierrehumbert, Phys. Rev. Lett. **57**, 2157 (1986).
[9] N. N. Mansour and S. L. Lundgren, Phys. Fluids A **2**, 2089 (1990).
[10] J.-P. Racz and J. F. Scott, J. Fluid Mech. **595**, 265 (2007).
[11] R. R. Kerswell, Geophys. Astrophys. Fluid Dyn. **72**, 107 (1993).
[12] H. P. Greenspan, *The Theory of Rotating Fluids* (Cambridge University Press, Cambridge, U.K., 1968).
[13] H. Poincaré, Bull. Astron. **27**, 321 (1910).
[14] R. J. Wiener, P. W. Hammer, C. E. Swanson, and R. J. Donnelly, Phys. Rev. Lett. **64**, 1115 (1990).
[15] P. Sagaut and C. Cambon, *Homogeneous Turbulence Dynamics* (Cambridge University Press, Cambridge, U.K., 2008).
[16] N. Leprovost and E.-J. Kim, Phys. Rev. E **78**, 016301 (2008).
[17] S. Leblanc and C. Cambon, Phys. Fluids **9**, 1307 (1997).
[18] C. Cambon, J-P. Benoit, L. Shao, and L. Jacquin, J. Fluid Mech. **278**, 175 (1994).
[19] A. Salhi and C. Cambon, J. Fluid Mech. **347**, 171 (1997).
[20] G. Ruediger, *Differential Rotation and Stellar Convection* (Gordon and Breach, New York, 1989).
[21] E.-J. Kim and N. Leprovost, Astron. Astrophys. **465**, 633 (2007).
[22] C. M. Bender and S. A. Orszag, *Advanced Mathematical Methods for Scientists and Engineers* (McGraw-Hill, New York, 1978).
[23] F. G. Jacobitz, in *Proceedings of the Fifth International Symposium on Turbulent Shear Flow Phenomena, Munich, 2007*, edited by R. Friedrich, N. A. Adams, J. K. Eaton, J. A. C. Humphrey, N. Kasagi, and M. A. Leschziner.
[24] D. Yu and S. S. Girimaji, J. Fluid Mech. **566**, 117 (2006).
[25] R. Rogallo, NASA Tech. Memo. No. 81315 (1981).
[26] F. G. Jacobitz, L. Liechtenstein, K. Schneider, and M. Farge, Phys. Fluids **20**, 045103 (2008).
[27] L. J. A. van Bokhoven, C. Cambon, L. Liechtenstein, F. S. Godeferd, and H. J. H. Clercx, J. Turbul. **9**, 1 (2008).
[28] L. Cesari, *Asymptotic Behavior and Stability Problems in Ordinary Differential Equations* (Springer-Verlag, Berlin, 1959).